(

FINAL
IN -34-CR
2cTT
45324
P. 26

FINAL TECHNICAL REPORT

Kinetics of Diffusional Droplet Growth in a Liquid/Liquid Two-Phase System

M.E. Glicksman, V.E. Fradkov,
Materials Engineering Department
Rensselaer Polytechnic Institute

January 1, 1995

Introduction

Precipitate aging in thin films is often characterized by mixed-dimensional coarsening, when 3-D precipitates interact through 2-D diffusion restricted to the film plane. Such processes can be physically modeled by arranging a distribution of liquid droplets embedded in an isolated fluid layer. The average size of the precipitated particles increases under the capillary driving force . Larger particles grow on account of the smaller ones which shrink and vanish. This process occurs in solids, liquids and even gases, having similar phenomenology and asymptotic scaling behavior. The mechanism of mass transfer among the particles is diffusion in the interparticle matrix space.

Although the driving force and mechanism of the process are well known, there are many additional factors making theoretical description of the coarsening difficult. One such factor is gravity. In a liquid or gas matrix with particles present having a different mass density gravity leads to sedimentation, *i.e.* settling of the particles rather than diffusion-limited coarsening. To prevent such sedimentation, experiments should be performed in microgravity. An alternative is to match the densities of the matrix and the particles as closely as possible.

A new powerful experimental technique based on holographic observations, developed at the NASA Marshall Space Flight Center, now permits observation of small liquid droplets coarsening. This technique was developed and used for mixed-dimensional coarsening studies by our co-investigators Drs. D.O. Frazier, W.K. Witherow, B.R. Facemire, J.P. Downey, and J.R. Rogers, of the Space Science Laboratory. Experiments were conducted on an isopycnic two-phase alloy of succinonitrile and water, annealed isothermally over a four-month period. The succinonitrile-rich droplets precipitate from a water-rich liquid matrix having a density very close to that of the droplets. The matrix and droplets, however, have different optical indices. The results of these experiments, along with the results of computer simulation based on the quasi-static diffusion approximation developed at Rensselaer are reported below. These results were published recently in [1, 2]. Copies of these papers are attached to this report (see Appendices I and II).

Experiment

The alloy selected for experiments exhibits total mutual solubility at relatively high temperatures, and a critical point and miscibility gap at lower temperatures. Small (10 to 50 μm) droplets with uniform shapes of spherical caps precipitate on the walls of the test cell. The isothermal annealing causes coarsening by diffusion among the droplets. The distance between the front and the back cell walls is 100 μm, which is smaller than a typical distance between the droplets. The boundary conditions at the walls impose a zero normal diffusion flux. Such a geometry and the boundary conditions imply that the diffusion field among the droplets may be considered as two-dimensional. For three-dimensional objects exchanging atoms by two-dimensional diffusion field, the dimensionality of the problem suggests the scaling behavior $\overline{R}^4 \propto t$, where $\overline{R}$ is a characteristic linear scale of the system, and t is the time [3]. For example, $\overline{R}$ may be chosen as the average radius of the droplets. Fig. 1 shows the average radius of the droplets *vs.* time. Because the total volume of the system is constant, $N\overline{R^3} = const$, where N is the number of droplets. The consequence of this scaling behavior is that the number of droplets N depends on time as $N^{-4/3} \propto t$ (see Fig. 2).
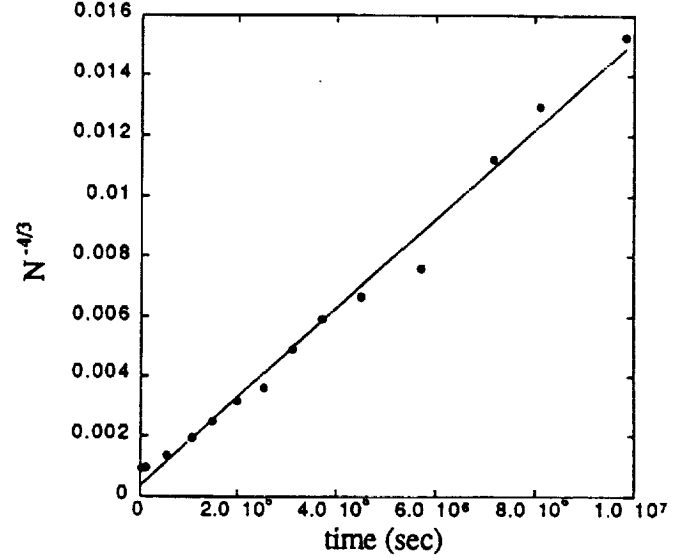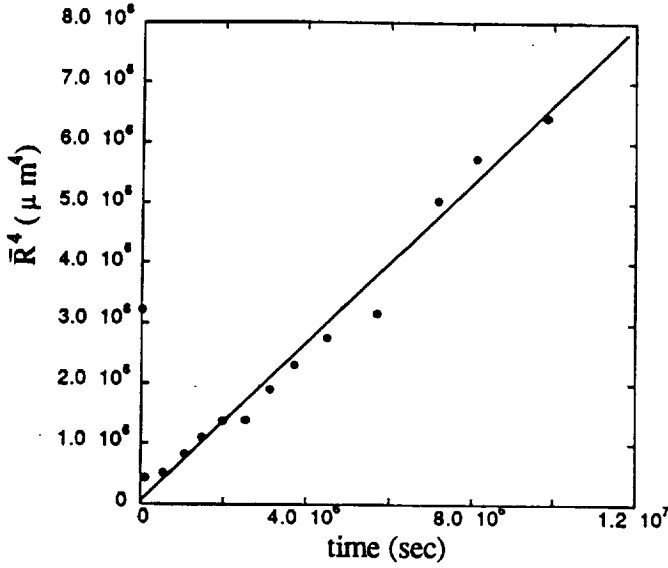
Fig. 1. Scaling of average droplet radius with time.   Fig. 2. Scaling of number of droplets with time.

The holographic experimental technique permits, for the first time, one to obtain trajectories (time dependencies of the particle size) for each individual droplet (see Appendix I). This information allows the direct comparison of experiment with the theoretical calculations.

Theory

General formulation

The theoretical analysis of coarsening of the droplets requires solving the moving boundary diffusion problem (Stefan problem) with boundary conditions at the test cell walls and at the surfaces of the droplets. The boundary condition imposed on the droplet surfaces is given by the Gibbs-Thomson equilibrium capillary equation

$$c(R) = c_0 \cdot \left(1 + \frac{2\gamma\Omega}{kT}\frac{1}{R}\right),$$

where $c(R)$ is the equilibrium concentration at the surface of the droplet with radius R, c_0 is the equilibrium concentration for a planar interface, γ is the surface tension, Ω is the atomic volume, k is the Boltzmann constant, and T is the temperature. For a large number of droplets, even a numerical solution of this extremely complex problem appears numerically unrealistic. However, if c_0 is much lower than the concentration inside the droplets then the characteristic diffusion time is much less than the time needed for significant change of the droplet radius. As a consequence, one can, following Todes [4], substitute the Lapacian equation $\nabla^2 c = 0$ for the diffusion equation, $\dfrac{\partial c}{\partial t} = D\nabla^2 c$. This concept of *quasi-stationary* diffusion was used later by Lifshitz and Slyozov [5], Wagner [6] and others in the formulation of classical coarsening theory.

Even after such a large simplification, the problem still remains too difficult for direct numerical analysis. Each droplet surface represents a continuum of sources/sinks for solute atoms. As the concentration field obeys the Laplacian equation, one can use the multipole series expansion for approximating the exact boundary conditions at the droplet surfaces. In two dimensions, the multipole series is given by

$$c(\vec{r}) = \bar{c} + q\ln r + \frac{\vec{d}\cdot\vec{r}}{r^2} + \ldots$$

The larger is the interdroplet distance as compared to the droplet radii, the fewer is the number of terms of the series needed. The logarithmic term is referred to as a "monopole" term, the next one as a "dipole" term, etc. It is important to mention that the rate of the droplet size change is defined by the monopole term alone:

$$\frac{\mathrm{d}}{\mathrm{d}t}R_i = -\frac{2\pi}{3\alpha}\Omega\cdot Dc_0 H\frac{q_i}{R_i^2},$$

where α is a geometrical factor depending on the contact angle, and H is the distance between the test cell walls.

Monopole Approximation

The general two-dimensional solution of the Laplacian equation in the monopole approximation is

$$c(\vec{r}) = \bar{c} - c_0 \sum_{i=1}^{N} q_i \ln \frac{|\vec{r}_i - \vec{r}|}{R_i},$$

where $\vec{r}_i$ and R_i are the position of the center and the radius of the i-th droplet, respectively, and N is the number of droplets. To obtain the values of $(N+1)$ constants of integration $\bar{c}$ and q_i we use the Gibbs-Thomson equilibrium boundary conditions at the particle surfaces. Neglecting the droplet radius as compared to the interdroplet distance one substitutes the position at the surface of the droplet by the position of its center. This procedure provides a linear set of N equations. The missing equation from the $N+1$ solution set corresponds to the boundary condition at infinity. In our treatment we used a mass conservation equation instead, which provides the last equation needed to determine the solution set (see Appendix II).

The monopole approximation provides the rates of the droplet radii change depending on the positions of the individual droplets. The values of q_i's are determined by the diffusion fields created at the vicinity of the i-th droplet by the other droplets. However, we neglect the size of the droplet compared to the interdroplet distance, resulting in the neglect of the gradients of the diffusion field. Note, that in two dimensions the monopole term changes very slowly, as a logarithmic function. The next term in the expansion is a dipole term accounting for the gradients in the vicinity of the droplets. This term decays as slowly as the reciprocal of the distance to the center of the droplet and, therefore, may be important in droplet systems with higher volume fractions.

Dipole Approximation

The general solution of the Laplacian equation incorporating the dipole terms is given by

$$c(\vec{r}) = \bar{c} + c_0 \sum_{i} \left(-q_j \ln \frac{|\vec{r} - \vec{r}_j|}{R_j} + \frac{\vec{d}_j \cdot (\vec{r} - \vec{r}_j)}{|\vec{r} - \vec{r}_j|^2} \right).$$

6

To satisfy the equilibrium boundary conditions for any direction of $\vec{R}_i$, the following two equalities have to be met:

$$\frac{2\gamma\Omega}{kT}\frac{1}{R_i} - c(\vec{r}_i) = 0,$$

and

$$\vec{d}_i = -R_i^2 \cdot \left.\frac{\nabla c}{c_0}\right|_{\vec{r}_i}.$$

Together with the mass conservation condition, this results in the full set of (3N+1) linear equations for q_i's, $\vec{d}_i$'s and $\bar{c}$ (see Appendix II).

During the numerical simulation, the set of ordinary differential equations for the droplets radii is solved using a fourth-order Runge-Kutta algorithm. The values of the q_i's are obtained at each time step by solving the corresponding linear set of equations for the monopole dipole approximation. The disappearance of a shrinking droplet causes a singularity to occur in the flux values. In order to deal with these singularities numerically, the time step is adjusted by estimating the shortest droplet lifetime. The droplets are eliminated from the calculation when they fall below the threshold size being much smaller than the average droplet size in the system at that instant. The entire numerical program was tested and verified using a two-droplet case permitting the analytical solution.

Results and Discussion

The initial state for the simulation is taken from the experimental data described above. To find the relation between the experimental time t and the computational dimensionless time τ we used the time dependence of the number of droplets shown in Fig. 2. The results of both monopole and dipole calculations fit the experiment well for some period of time. The deviations observed for larger times might result from the accumulated influence of the droplets located beyond the experimental field of view. As we already mentioned, in two dimensions the dependence of interaction between the droplets on the distance is rather subtle, and the interacting particles are not required to be located close to each other.

7

In contrast with the global behavior for the droplet population, the results of the comparison between the experiment and the calculations for *individual* droplet evolution vary widely. In many cases we observe good agreement between the experiment and both dipole and monopole approximations, as shown in Fig. 3. In some cases the dipole calculation deviates from the monopole calculation and the dipole results are closer to the experimental measurements (see Fig. 4). In the third group we find large deviations between the calculations and the experimental results (see Fig. 5). We suggest that the cases in which the dipole calculation results diverge from the monopole calculation the diffusion field contains a strong gradient at the vicinity of the droplets. The cases with poor agreement between the calculations and the experiment appears to be caused by the uncontrollable influence of the droplets located beyond the experimental field of view.
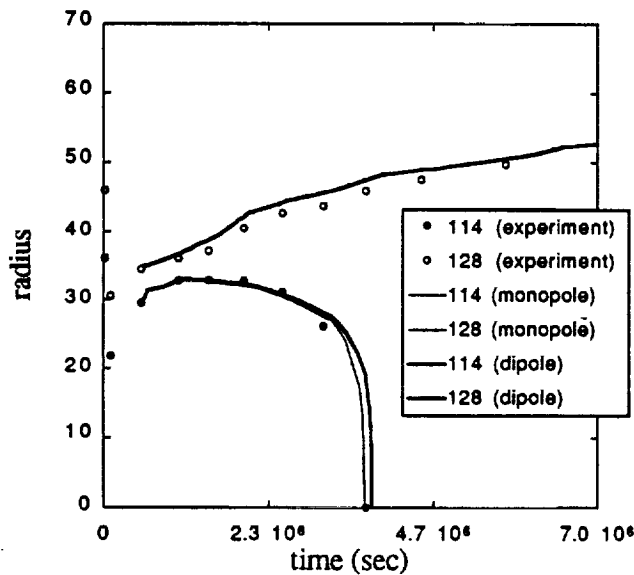

Fig. 3. Typical individual droplet evolution in the case of a good agreement between the experiment and the calculations
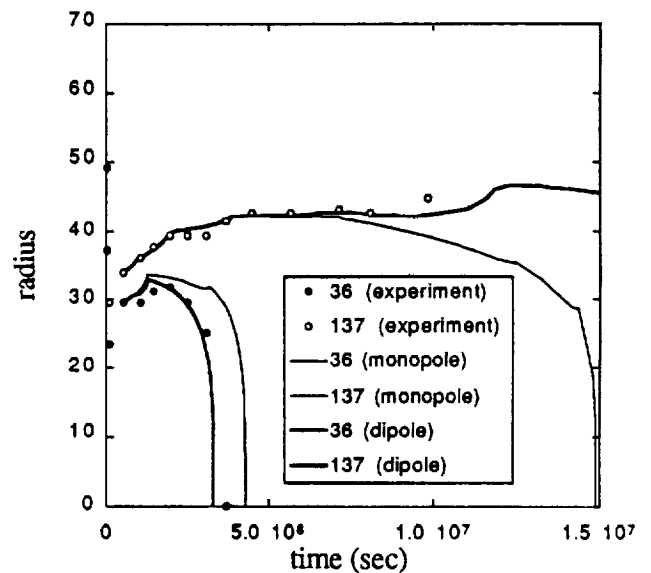
Fig. 4. Typical individual droplet evolution in the case when the dipole approximation shows better agreement with the experiment as compared to the monopole approximation.
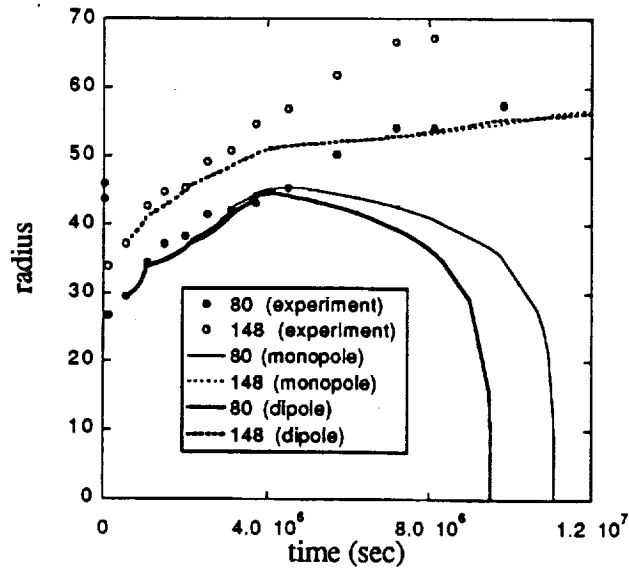
8

Fig. 5. Typical individual droplet evolution in the case of a bad agreement between the experiment and the calculations

References

1. J. R. Rogers, *et al.* *J. of Electronic Materials*, 23(10), 841 (1994).

2. V. E. Fradkov, *et al.* *J. of Electronic Materials*, 23(10), 849 (1994).

3. W. W. Mullins. *J. Appl. Phys.*, 28(3), 333 (1957).

4. O. M. Todes. *J. Phys. Chem (Sov.)*, 20(7), 629 (1946).

5. I. M. Lifshitz and V. V. Slyozov. *J. Phys. Chem. Solids*, 19 35 (1961).

6. C. Wagner. *Z. Electrochem.*, 65 581 (1961).

Appendix 1

Coarsening of Three-Dimensional Droplets by Two-Dimensional Diffusion: Part I. Experiment

J.R. ROGERS

National Research Council, Space Science Laboratory, NASA Marshall Space Flight Center, Huntsville, AL 35812

J.P. DOWNEY, W.K. WITHEROW. B.R. FACEMIRE, and D.O. FRAZIER

Space Science Laboratory, NASA Marshall Space Flight Center, Huntsville, AL 35812

V.E. FRADKOV, S.S. MANI, and M.E. GLICKSMAN

Rensselaer Polytechnic Institute, Troy, NY 12180-3590

An experimental study of diffusional coarsening, or Ostwald ripening. in a liquid-liquid two-phase system is described. An experiment performed at its isopycnic point, 42°C, allowed observations for the long times required to investigate coarsening. A holographic technique was instrumental in this work. Holograms taken *in situ* permit investigation of details regarding both the influence of local environmental conditions on individual droplet size histories and measurement of global averages. This study utilized a 100 μm pathlength test cell. The discrete phase was nucleated on one wall of the cell. This configuration resembles island formation in thin film growth. Observation of Ostwald ripening over a period of 1×10^7 s (~4 mo.) reveals that droplet number decays as $t^{-0.733}$ and the average radius increases as $t^{-0.247}$, in the asymptotic limit. This shows good agreement with theoretical predictions for diffusional growth of spherical caps on a two-dimensional substrate which is a valid approximation for the geometry of this experiment. Part I of this paper describes the experimental results. Part II discusses a numerical model for droplet growth in a comparison with the experimental results.

Key words: Diffusion, holography, kinetics, microstructure coarsening. Ostwald ripening, phase transformation

INTRODUCTION

Ostwald ripening is the process by which larger droplets grow at the expense of smaller ones, by diffusion of mass away from droplets below a critical radius toward ones above this critical size. The phenomenon is important in many disciplines. Of particular interest to materials processing is its influence on the time dependence of droplet (or particle) size distributions of a precipitated phase.

The objective of this work was to perform an experimental study of the development of microstructures and the growth of a second phase in a two-phase system. To a large extent, growth and distribution of the discrete phase determine the mechanical and electronic properties of an alloy. A detailed understanding of microstructure is essential to predicting the behavior of a material. For example. the formation and growth of clusters in semiconductor thin film deposition result in microstructures which dictate film properties in a device application. Most modeling and experimental studies focus on the average particle and the late stages of growth processes. However, the behavior of the "weakest link" rather than an average property is fundamental to developing predictability regarding practical problems such as fracture analysis in metal fatigue. The unique capabilities provided by holographic tech-
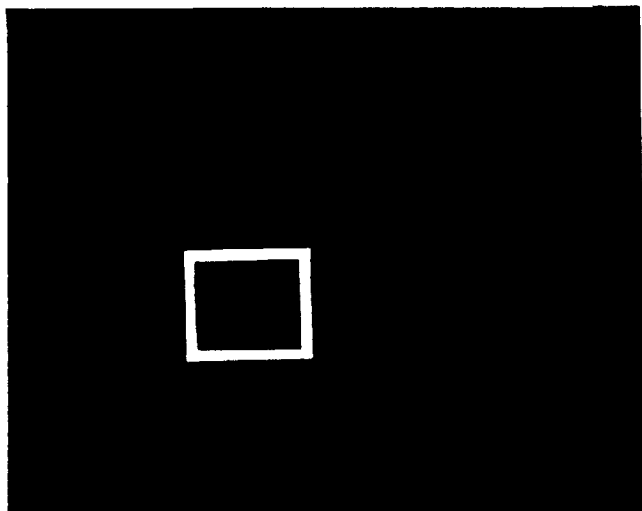
Fig. 1. Projected image of the test cell. The white box indicates the area selected for analysis.
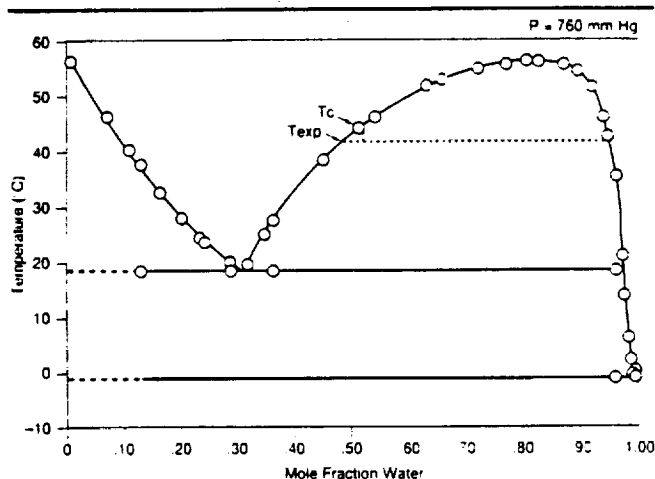

Fig. 2. Succinonitrile/water phase diagram; T_c and T_{exo} represent the consolute and experiment temperatures, respectively.

niques allow detailed analyses of both local dynamic behavior within the context of a particle ensemble and resulting microstructures from a statistically significant population.

The theoretical analysis of coarsening of the droplets requires solving the moving boundary diffusion problem (Stefan problem) with boundary conditions at the test cell walls and at the surfaces of the droplets. The boundary condition imposed on the droplet surfaces is given by the linear form of the Gibbs-Thompson equilibrium equation

$$c(R) = c_0 \left(1 - \frac{L}{R} \right),$$ (1)

where $c(R)$ is the equilibrium concentration at the surface of the droplet with radius R, c_0 is the equilibrium concentration at the plane interface, and L is the Gibbs-Thompson characteristic length, given by
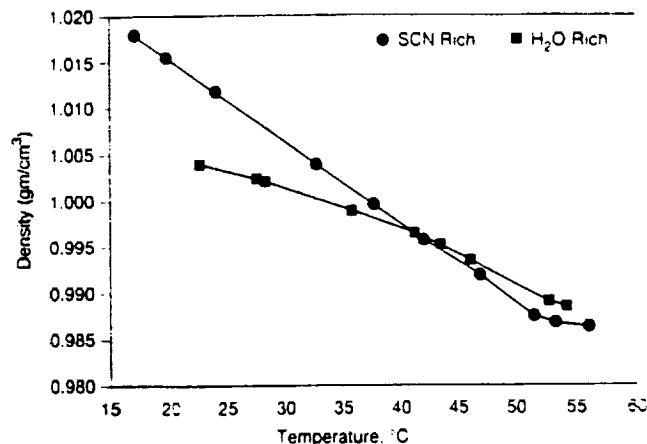
$$L = \frac{2\gamma\Omega}{kT},$$ (2)

Fig. 3. Densities of equilibrium phases in succinonitrile/water as functions of temperature.

where γ is the interfacial tension, Ω is the molecular volume, k is the Boltzmann constant, and T is the temperature.

In their classical studies of the ripening process Lifshitz, Slyozov, and Wagner (LSW)[1,2] and Todes[3] applied the steady state approximations to the diffusion process. This approximation is valid for the case of very low supersaturation where the characteristic diffusion time is much less than the time required for a significant change in the droplet radius. Using this approach, they determined global scaling laws for the case of three-dimensional diffusion processes. The length scale for the ripening process can be considered to be the average droplet size which predictably grows as $t^{1/3}$ for the latter stages of a three-dimensional diffusional growth. The decrease in the number of droplets as a function of time for the three dimensional case is given by $N(t) \propto t^{-1}$.[1,2] Experimental investigations and numerical simulations support this scaling prediction.

Ripening processes follow different scaling laws in a two-dimensional system. An example of this is the growth of spherical caps on a two-dimensional substrate. Theoretical arguments by Chakraverty for multiparticle diffusion between three-dimensional particles with mass transport restricted to two-dimensions predict $N(t) \propto t^{-3/4}$ and that length scales as $t^{1/4}$.[4] Slyozov obtained the same result for interacting three-dimensional clusters located on a planar substrate.[5] Both Chakraverty and Slyozov utilized the mean-field approximation for their two-dimensional concentration field and assumed implicitly a low volume fraction of droplets. Their prediction has been observed experimentally.[*] Part II of this paper describes the development of a numerical model of three-dimensional droplet growth due to two-dimensional diffusion.

This study employed holography to record the ripening processes in the experimental test cell. The holograms, permanent records of the wavefront, may be reconstructed and the wavefront precisely reproduced. The reconstructed wavefront gives an exact three-dimensional reproduction of the test cell con-

tents at the instant of exposure. Each hologram allows measurement of all the droplet radii in the test cell at a given instant of time. During reconstruction, the hologram image can be moved with relative ease, and the entire test cell volume can be investigated by stepping the field-of-view through a magnified reconstructed image of the test cell. A square region consisting of 25 fields of view (about 5% of the recorded test cell volume), initially populated with 187 droplets, comprised the area selected for analysis. Figure 1 shows a projection of the test cell indicating the area chosen for detailed analysis. It is important to note that the holographic records archive a great deal of additional data.

MATERIALS AND METHODS

All theoretical models of the Ostwald ripening consider growth only due to diffusion. A test of this theory required an experiment devised to study nearly pure diffusional growth by simultaneously eliminating coalescence and convection. Solutions of succinonitrile/water (SCN/H$_2$O) offer an experimentally convenient model system for the study. Figure 2 shows the phase diagram for SCN/H$_2$O.[7] Above the critical consolute temperature, 56°C, SCN/H$_2$O forms a single phase. When compositions spanning the miscibility gap of the phase diagram are cooled through the coexistence curve, the system separates into droplets of one liquid dispersed in another. Unlike metallic alloys, both the droplet and surrounding phases are transparent, and the growth of the former may be followed by optical means in situ. Moreover, because the phase separation occurs near room temperature, elaborate furnaces for temperature control are not required as would be the case for metals. These experiments were performed near the isopycnic temperature of approximately 42°C (Fig. 3). The droplets were located on the inside wall of a 100 μm pathlength optical cell. During the observation period which spanned about four months, the droplet positions remained unchanged.

The SCN/H$_2$O system is well characterized as a transparent model for observations of metallic monotectic solidification phenomena[8] and, therefore, was the system of choice for the Ostwald ripening studies. Succinonitrile was vacuum-distilled twice at a measured pressure of 10–20 mm Hg. Water was distilled and filtered through a Millipore Milli-Q water system giving a resistivity of 18 Mohm cm. Approximately equal volumes of the two components were mixed in a waterjacketed separatory funnel and allowed to equilibrate at about 45°C. Aliquots of the water-rich phase extracted from this solution, when cooled at 42°C, resulted in SCN-rich droplets. This phase was selected to assure that the nucleating phase would not wet and spread on the quartz test cell walls. Figure 4 shows nonwetting SCN-rich droplets on a quartz plate.

Experiment Test Cell and Apparatus

A commercially available micro cylindrical spectrophotometer cell shown in Fig. 5 having an optical path

length of 100 μm yielded particle densities low enough to allow holographic imaging with good resolution.[7] A 6 in. length of glass tubing attached to the cell fill port permitted sealing. Filling the cell consisted of extracting the lower phase from the reservoir thermostated at 45°C in a heated pipette, wiping the pipette to remove excess upper phase, and expelling the solution into the cell, while maintaining homogeneity by gently heating the pipette with a hot air gun. After the filling operation, the glass extension tube was sealed. Submerging the cell body in an ice bath prevented the solution from significantly changing composition due to vaporization during the sealing procedure. Heating the cell to 46°C for 48 h prior to the experiment assured solution homogeneity. The cell was transferred to the isothermal test chamber held at 46.4°C. Scattering of the laser light during a slow quench determined the actual consolute point to be 45.01°C. After reheating to 46.3°C for 24 h, stepwise quenching into the miscibility gap initiated the experiment. Observations taken during the quench assured the low volume fraction of discrete phase required for optical resolution considerations and for comparison to theory. A test chamber temperature of 42.5°C, close to the neutral buoyancy temperature, yielded an
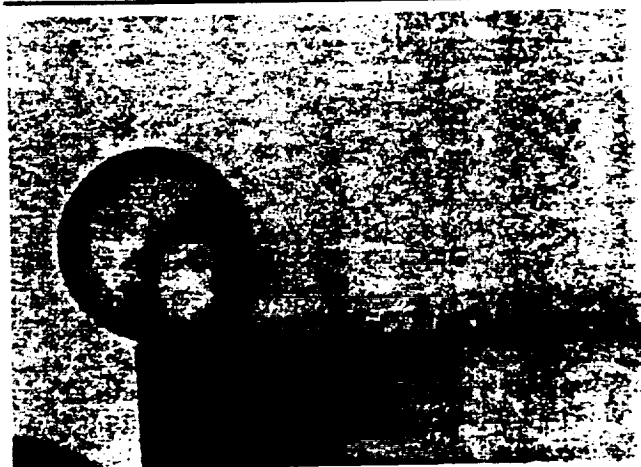
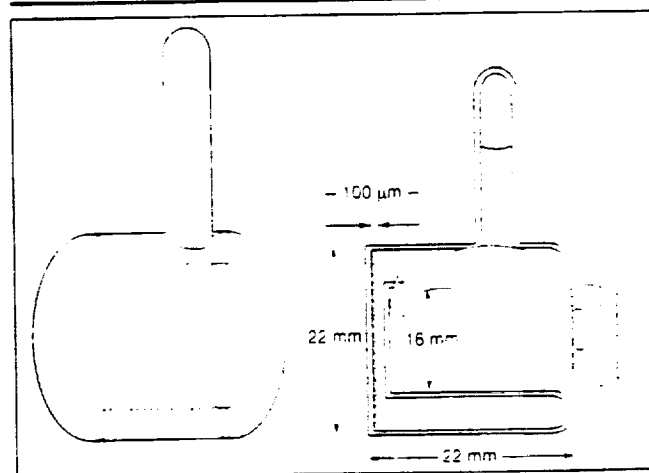Fig. 4. Photograph of succinonitrile-rich droplet on quartz.

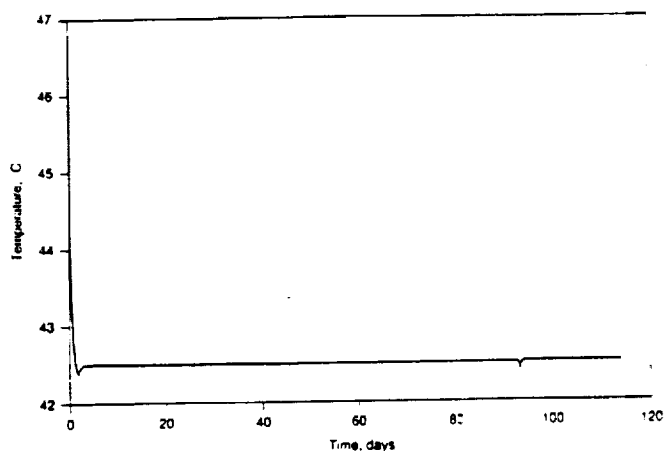Fig. 5. Test cell schematic showing nucleated droplets on the front wall of the cell

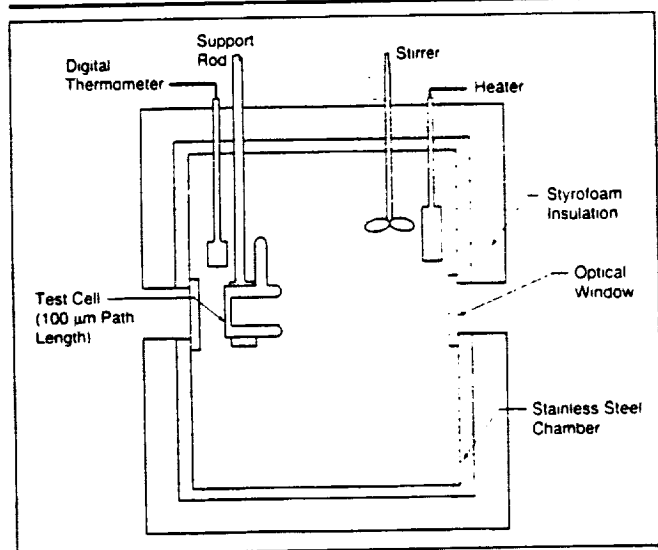Fig. 6. Temperature history for the duration of the experiment.

Fig. 7. Schematic of isothermal test chamber.

appropriate volume fraction and good thermal control. The temperature profile for the duration of the experiment is shown in Fig. 6.

Figure 7 is a schematic of the experimental apparatus. The test cell is positioned in a temperature-controlled water bath, an insulated stainless steel chamber with optical windows. A 0.2 μm filter element removed particles from the bath water that would interfere with holographic images. A thermistor in the bath was one leg of a ESI Model 250DE Wheatstone bridge and served as the feedback mechanism to provide control to a resistance heater in the bath. A Brookfield counter-rotating stirrer provided adequate stirring without entraining air in the water. Using this system, temperatures in the bath were controlled to 0.030°C over 94% of the experiment and 0.002°C for the first week of the 112-day observation. Performing the experiment near the isopycnic temperature minimized the effects of buoyancy.

Holographic Data

The time interval between holograms was initially 2 min. As the rate of change in droplet size distribu-

tion decreased, the time interval between holograms increased to two per day and finally to one per day. Each hologram is a record of the wavefront received by the film and contains all the optical information from the test cell for the instant in time when that hologram was made. When the hologram is reconstructed, the entire volume between the optical flats of the cell can be examined using various optical analysis tools which were not compatible with the test cell *in situ*. Details regarding the holographic construction and reconstruction systems can be found in Witherow[9] and Witherow and Facemire.[10] This holographic system gives a resolution of about 5 μm for the reconstructed image.

Reconstructed images from the holograms projected on the lens of a Dage MTI 70D video camera provided input for image analysis. The number of video fields required to span the diameter of the test cell in the reconstructed image and measurement of the test cell diameter determined the magnification factor for video-based droplet measurements. Using this magnification, the image of a single field comprised an area of 552×407 μm. Although the entire volume is available for study, the investigation examined a representative region of the test cell indicated in Fig. 1. One aim of this investigation, exploration of local interparticle interactive effects on the ripening processes, dictated use of contiguous rather than random fields. A 5 by 5 field section (25 fields), 5.617×10^6 μm^2, represents a volume of 5.617×10^4 cc, approximately 5% of the observable volume located within the optical viewing area of the test cell. Virtually all droplets focus in the same plane, indicating that they are located in the same plane. Further, they do not move at all over the lengthy duration of the experiment, indicating attachment to the same wall of the cell. This is to be anticipated because during the quench, the front wall of the test cell experienced the cooler temperature first because of reduced cooling fluid circulation on the sheltered back wall (Fig. 5). The stagnant fluid in the sheltered portion of the test cell cooled more slowly than the front wall. Therefore, droplets nucleated on the cooler, front face of the test cell.

RESULTS AND DISCUSSION

Of the 152 holograms obtained during the experiment, the first 25 were taken as the cell cooled to the operating temperature. 42.5°C. The remaining holograms at this temperature, clearly show the ripening of the droplet phase over time. Figure 8 shows a series of photographs from reconstructed holograms. The data reported here reflect measurements taken from 14 of the 152 holograms, selected at intervals spanning the duration of the experiment. Table I lists the hologram number and recording time for each hologram studied. Recording time indicates time elapsed since initiation of the quench sequence.

Calculations using density data of compositions (majority phase, 93 mole% H$_2$O; minority phase. 48 mole% H$_2$O) taken from the phase diagram tie line at the experiment operating temperature indicate a

volume fraction of the succinonitrile rich droplet phase of approximately 2.75%. The emphasis of this study is the evolution of a droplet size distribution due to diffusional growth. Therefore, quantitative analysis of this long-term growth process could not begin until the volume fraction of the discrete phase became constant. Figure 9 shows the volume of the droplet phase in the viewing volume as a function of time. Calculation of total droplet volume assumes uniform shape for the droplets. This approximation is consistent with observations of wetting of succinonitrile-rich phase on quartz as shown in Fig. 4. Figure 9 indicates that the constant volume condition is attained by the second observation (1.2 days). Once constant volume is achieved, the average total volume of the droplet phase within the viewing volume did not exceed 1.4×10^{-5} cm^3, the maximum deviation from this value is 5%. This corresponds to a maximum volume fraction of 2.5%. This is, within the limits of experimental error, in good agreement with the volume fraction of 2.75%, calculated from the phase diagram.

Theoretical analysis of ripening processes generally considers the long-time asymptotic behavior. Figure 10 is a plot of the number of droplets within the field of view as a function of time. Linear regression performed on the observations indicates that in the later stages of the experiment, the slope of the curve achieved a value of −0.733, with a correlation coefficient of 0.994. The geometry of our experiment is represented by spherical caps located on a substrate interacting through two-dimensional diffusion fields, as indicated in Figure 5. Chaklaverty[4] developed expressions for growth of a discrete phase of spherical caps on a two-dimensional substrate due to surface diffusion. His analysis indicates that N scales as $t^{-3/4}$. Our experimental results for the rate of droplet decay are in good agreement with this value.

Figure 11 shows the change in average droplet radius as a function of time. During the reported period of observations, a 138% increase in average radius is realized. The analysis of Chakraverty[4] predicts that r scales as $t^{1/4}$ in the asymptotic limit. The

plot of r vs time shown in Fig. 12 reveals that in the asymptotic limit (after ~2.5 weeks) the slope of the best fit line through these data is 0.247 with a correlation coefficient of 0.986. Again, our experimental data show agreement with the trends predicted by theory.

Statistically, self-similarity is a hallmark of the Ostwald ripening effect.[1,2,6] Theoretical analysis shows

Table I. Numbers and Recording Time for Studied Holograms

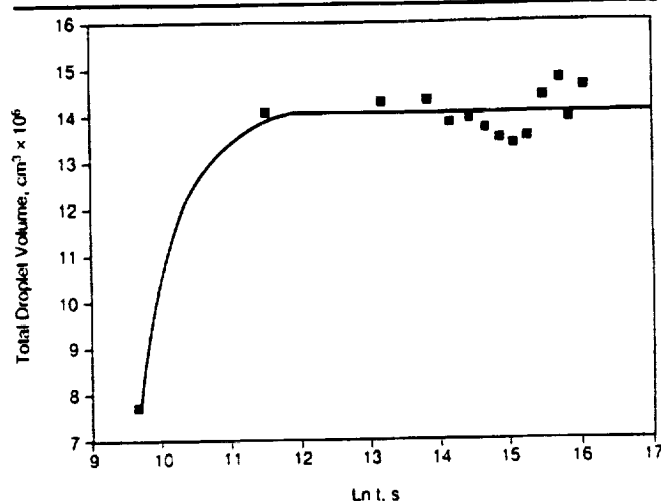| Hologram Number	Time, Seconds
20	1.6×10^4
30	1.06×10^5
40	5.4×10^5
50	1.07×10^6
61	1.5×10^6
70	2.0×10^6
80	2.5×10^6
90	3.1×10^6
100	3.7×10^6
110	4.5×10^6
120	5.7×10^6
130	7.2×10^6
140	8.1×10^6
152	9.8×10^6

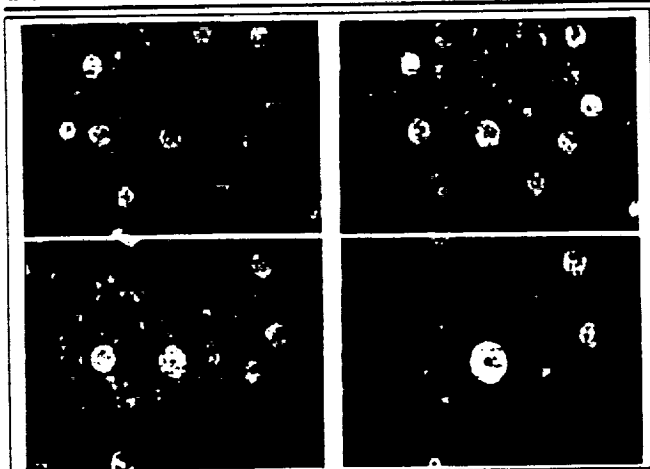Fig. 9. Total droplet volume as a function of time.

Fig. 8. Photographs from four holograms of the same field-of-view which show ripening effects over a period of several months.
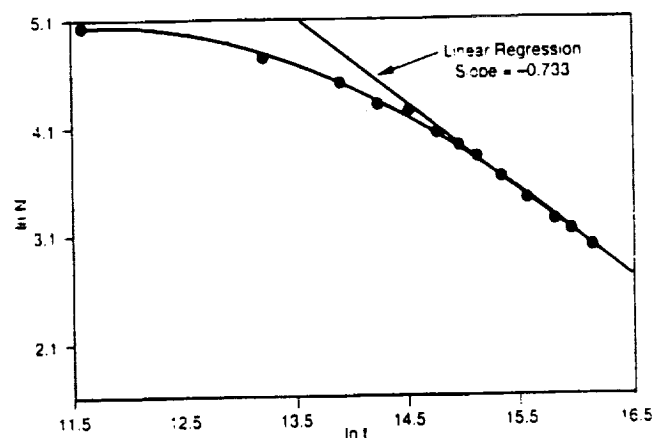

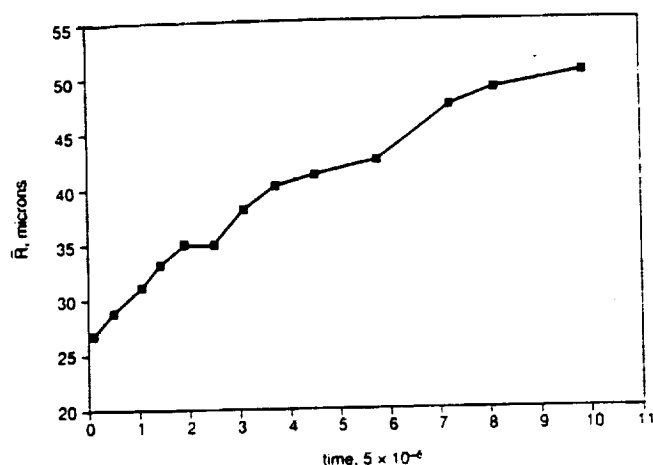Fig. 10. Number of droplets in the selected area as a function of time.
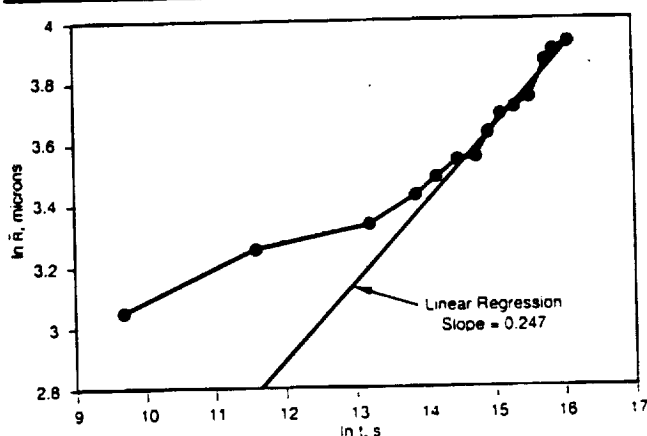
Fig. 11. Average radius as a function of time.

Fig. 12. Ln average radius as a function of Ln time.

that a scaled-time-independent droplet radius distribution function exists.[6,11] Morphological configurations during Ostwald ripening should remain statistically equivalent when examined under appropriately scaled magnifications. Figure 13 shows photographs taken directly from selected holograms during the ripening experiment. Photographs were taken to show a large portion of the test cell contents (approximately 50% of the area shown in hologram 151, or 1.08 cm²). It is important to note that the droplets create interference fringes on these pictures. Droplets are the bright spots surrounded by the halo-like interference fringes. Additionally, bright spots occur inside the small droplets, which act as lenses. The magnification factors have been scaled with the average droplet radii. The photographs show very similar size distribution characteristics. Quantitative assessment of statistical self-similarity requires a great deal of additional data. Efforts to measure the size histories of additional droplets are presently under way.

Holography enables the study of local environment effects on the rate of droplet growth. Figure 14 shows the droplet size history of a centrally located portion of the viewing region in the vicinity of Field 19. Asterisks denote locations of droplets consumed due to the ripening process. Field 19 contained droplets 141–146. Figure 15 is a plot of the droplet diameters

by hologram number. Note that the curve for droplet 145 intersects the curves for droplets 143 and 141. Classic ripening theory predicts that the larger droplets in a population should grow; the individual droplet trajectories should not cross. A careful examination of Fig. 14 reveals that droplet 145's spatial location favors diffusional interactions with droplet 171 in Field 23; droplet 145 shrinks and eventually disappears due to local effects.

Local effects also become evident in an examination of the critical radius. The critical radius at a given time in the experiment can be considered that droplet size at which there is no net flux of material to the droplet, where dR/dt = 0.00. Figure 16 shows plots of rate of change of droplet radii for selected holograms during the ripening stage of the experiment and the value of R_c predicted by theory. Theory suggests a single value for the critical radius given by

$$R_c(t) = \frac{9}{8}\overline{R}(t).$$

Examination of Fig. 16 reveals no observable rate of change in droplet radius for a range of values of droplet radii. The local environment of each specific droplet determines the critical radius within that environment. This range of values could be considered "microstructural fluctuations" and indicates the range of deviations from theoretical predictions. It is also evident that, within the resolution of the method, droplets of the same size appear to grow and shrink over the same time interval. This range of deviations may be a better predictor of the ultimate properties and function of the material in applications than the theoretical value of the "global critical radius."

CONCLUDING REMARKS

This study demonstrates limitations of mean field approaches which adequately predict scaling laws but not local droplet behavior during Ostwald ripening. Mean field theories incorporate use of a screening length (often suggested as l_{sc} = 2 droplet radii). Droplets spaced farther apart than that distance should grow or shrink only in response to differences between the concentration of the diffusing species at the surface of the droplet as defined by the Gibbs-Thompson equation and the mean field concentration. There is no direct interdroplet communication at distances which exceed l_{sc}. Therefore, where the interdroplet spacing exceeds ≈2 radii, all droplets larger than R_c should grow, all those smaller than R_c should shrink. Additionally, droplets of the same size should change size at the same rate. Data from this experiment indicates otherwise. The mean field approach is not sufficient to describe the behavior of individual droplets. Droplet interactions must occur in a more direct manner than suggested by the simple mean field approach.

In order to explore direct droplet interactions, the behavior of droplets with respect to size was examined. Surprisingly, the data includes observations in which droplets larger than their nearest neighbor
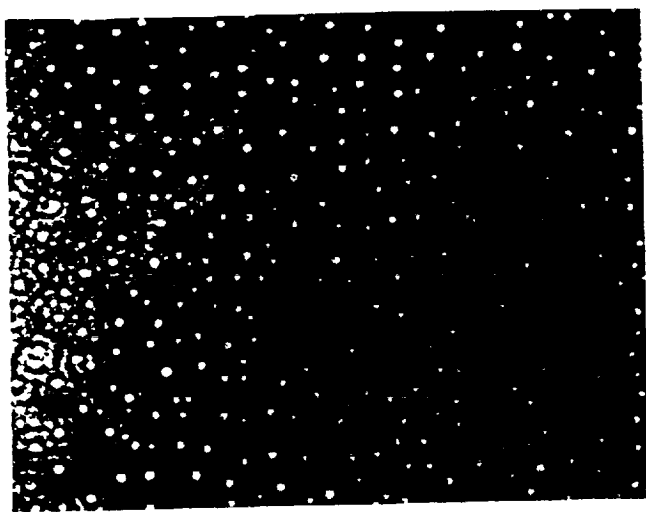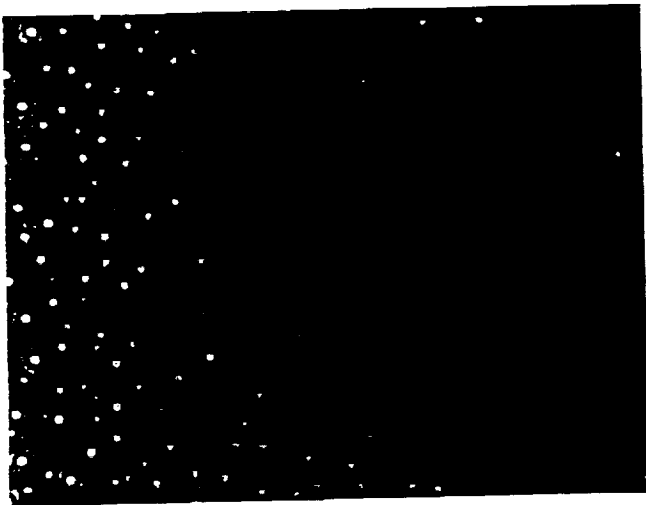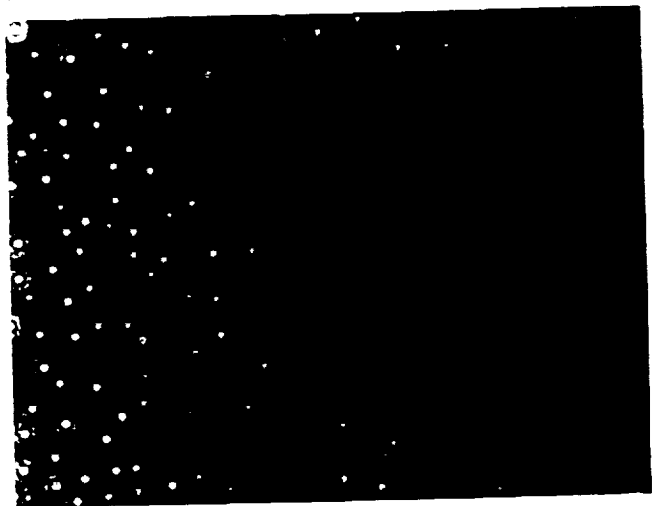
Fig. 13. Photographs of test cell at variable magnification for selected holograms: (a) HG 90, t = 3.1 × 10⁶ s; (b) HG 100, t = 3.7 × 10⁶ s; (c) HG 120, t = 5.7 × 10⁶ s; (d) HG 151, t = 9.8 × 10⁶ s.

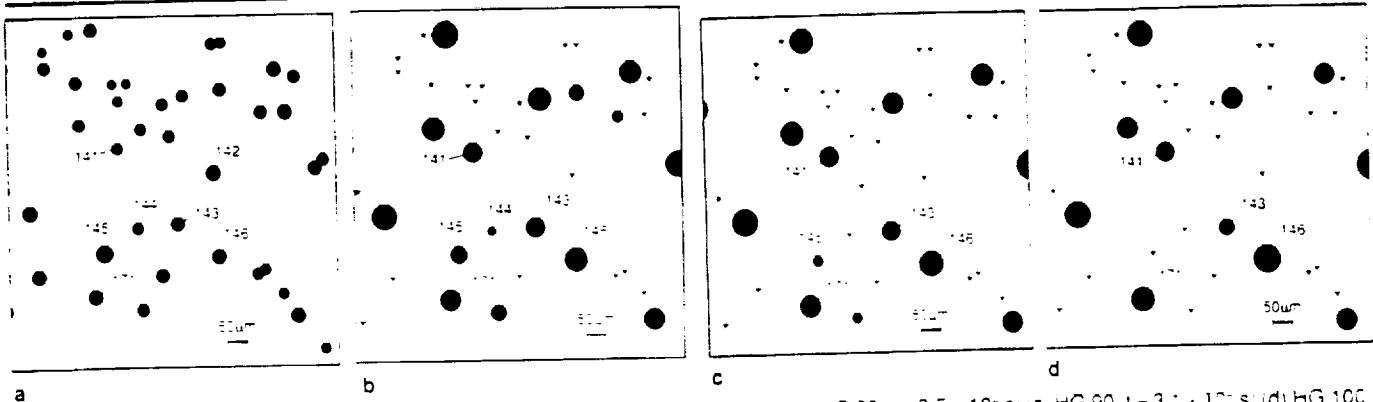
Fig. 14. Representation of droplets located near Field 19: a — HG 20, t = 1.6 × 10⁴ s; (b) HG 80, t = 2.5 × 10⁶ s; (c) HG 90, t = 3.1 × 10⁶ s; (d) HG 100, t = 3.7 × 10⁶ s

shrunk, and droplets smaller than their nearest neighbor grew. Clearly, these droplets were responding to the influence of droplets other than their nearest neighbor. The data suggests that the drop-size histories of individual droplets depends greatly on the details of the local environment. The simple approach of observing the interaction between a droplet and its nearest neighbor quickly becomes complicated when that nearest neighbor has another neighbor which is closer in another direction. The effects of the local

Rogers. Downey. Witherow. Facemire. Frazier. Fradkov. Mani, and Glicksman
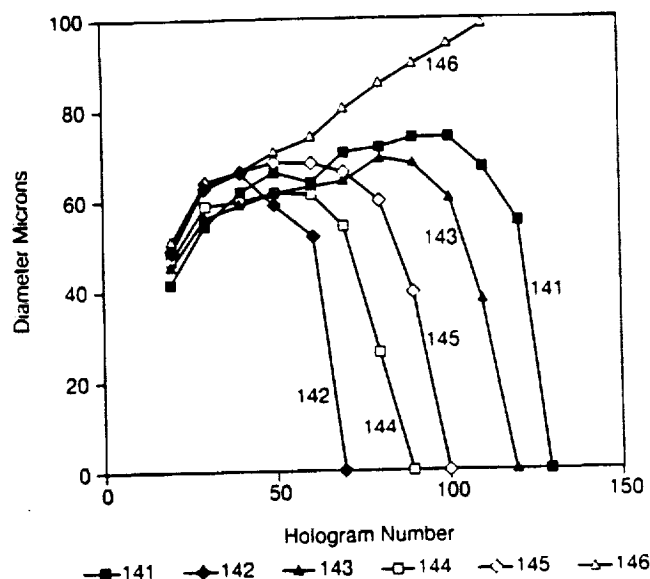
1006

Fig. 15. Individual droplet lifetime trajectories.

environment on the behavior of a specific droplet are subtle. Understanding requires the application of modeling techniques which can account for the nature of diffusional interactions of the droplets in the ensemble. An additional complicating factor which is not addressed in the present studies is the possible effects of residual concentration nonuniformities as droplets become smaller than the resolution of the observation system. Droplets of less than approximately 2–3 μm are below these limits.

This study also exemplifies the benefits of holography. Using conventional microscopy, only one field-of-view would be accessible during a given instant in time. Holographic microscopy allows reconstruction of the test cell image and extraction of full details regarding the local environment of a given droplet. Future plans include the application of phase shifting interferometry to the holograms of the experiment in order to determine the concentration field in the test cell. Direct assessment of the concentration field should greatly enhance the understanding of diffusive growth processes.

Computer modeling provides an important bridge between theoretical predictions and experiments. Part II of this paper describes computer modeling studies which examine multiple droplet interactions to account for the observed local effects. The model includes droplet interaction parameters for the entire ensemble of droplets observed during this experiment. Predictions from the model are compared to experimental observations reported in this paper.

ACKNOWLEDGMENT

REFERENCES

a

b
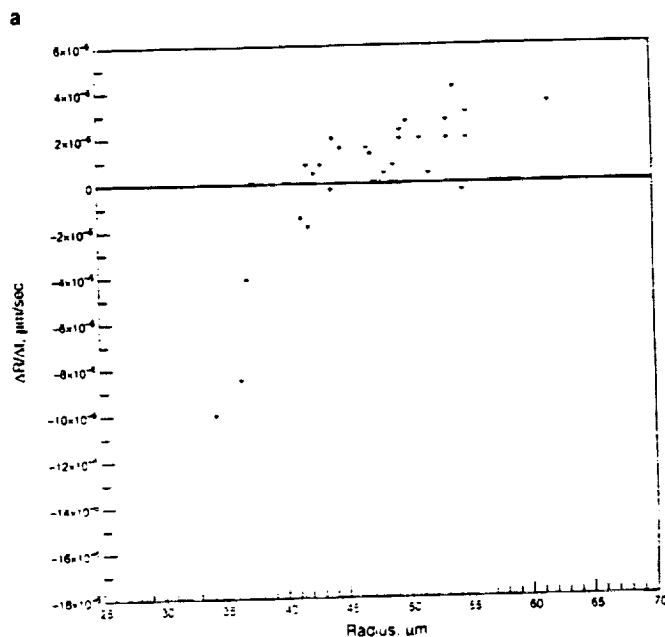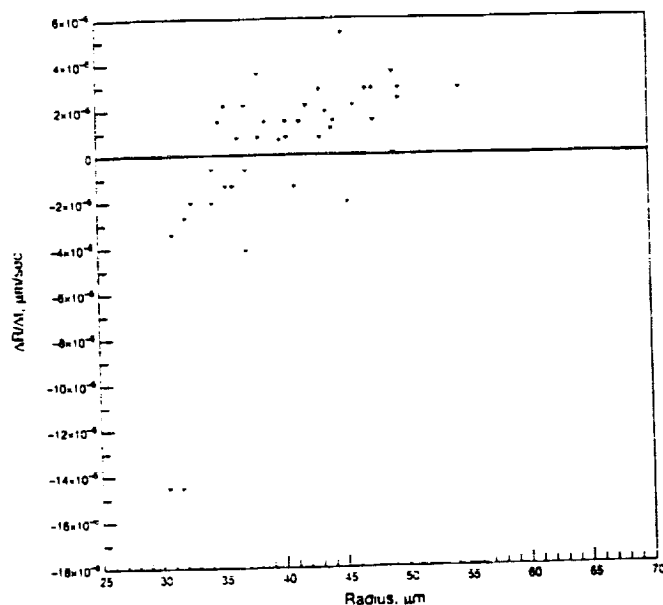
Fig. 16. Rate of change for droplet radii for holograms for selected intervals: (a) HG 100–HG 11; (b) HG 120–HG 130.

1. I.M. Lifshitz and V.V. Slyozov. *J. Phys. and Chem. of Solids* 19, 35 (1961).

2. S.C. Wagner. *Z. Electrochemic* 65. 581 (1961).
3. O.M. Todes. *Zh. Fis. Khim. 'Sov. J. Phys. Chem.*, 20. 629 (1946).
4. B.K.Chakraverty. *J. Phys. Chem. Solids* 28, 2401 (1967).
5. V.V. Slyozov. *Fis. Tverd. Tela* 9. 927 (1967).
6. M. Zinke-Allmany. L. C. Feldman and M. H. Grabow, *Surface Science Reports: A Review Journal* 16 (5). 377 (1992).
7. J.E. Smith. D.O. Frazier and W.F. Kaukler, *Scripta Met.* 18. 677 (1984).
8. D.O. Frazier and B.R. Facemire. *Thermochimica Acta.* 145. 301 (1989).
9. W.K. Witherow. *SPE* 18. 249 (1979).
10. W.K. Witherow and B.R. Facemire. *J. Colloid Interface Sci.* 104. 185 (1985).
11. P.W. Voorhees. *Ann. Rev. Mater. Sci.* 22. 197 (1992).

Appendix 2

Coarsening of Three-Dimensional Droplets by Two-Dimensional Diffusion: Part II. Theory

V.E. FRADKOV, S.S. MANI, and M.E. GLICKSMAN

Rensselaer Polytechnic Institute, Troy, NY 12180-3590

J.R. ROGERS

National Research Council, Space Science Laboratory, NASA Marshall Space Flight Center, Huntsville, AL 35812

J.P. DOWNEY, W.K. WITHEROW, B.R. FACEMIRE, and D.O. FRAZIER

Space Science Laboratory, NASA Marshall Space Flight Center, Huntsville, AL 35812

Theoretical modeling of coarsening among a finite cluster of precipitates is implemented, using the multipole expansion method. This method requires the diffusion field to behave quasi-statically. Two approximate solutions were developed, one to monopolar order, and other to the dipolar order. The conventional Gibbs-Thomson equilibrium relationship was used as the boundary condition at the precipitate-matrix interface. Part I of this paper considers a liquid-liquid system in a mixed-dimensional geometrical configuration, wherein three-dimensional precipitates interact via a diffusion field constrained in two dimensions. This kind of geometric configuration is often encountered in island evolution dynamics and phase segregation in thin films. The initial experimental configuration of droplets provides the initial condition for the simulation. Both monopole and dipole approximations closely follow the experimentally observed scaling laws, characteristic for the mixed-dimensional coarsening ($N^{-4/3}$ and $\bar{R}^{4}$, varied linearly with time, where N is the number of droplets in the experimental field of view, and $\bar{R}$ is the average droplet radius). Good agreement is observed for time evolution of radii of some individual precipitates. Certain deviations appearing among the two approximate solutions and the experimental data are discussed.

Key words: Coarsening, kinetics, microstructure coarsening, Ostwald ripening, phase transformation, quasi-stationary diffusion

INTRODUCTION

Phase coarsening is an important process in the microstructural evolution of dispersed multiphase systems. The initial excess interfacial free energy of such a system is elevated due to the large number of precipitated particles with high curvatures. During coarsening, the excess interfacial energy is reduced via diffusional mass transfer from regions of higher average curvature to regions of lower curvature. The average size of the precipitated particles increases with time, and the total number of particles in the system decreases. Larger particles tend to grow at the expense of the smaller ones which shrink and vanish. This process, whether occurring in solids, liquids, or even gases, has similar phenomenology and asymptotic kinetic scaling behavior. In the case considered here, the mechanism of mass transfer among the particles is diffusion in the interparticle space (matrix).

Part I of this paper[1] presents details of the droplet coarsening experiments, where a holographic technique is used to observe *in situ* the size and position of each individual precipitate in an isopycnic (neutral

Fradkov. . ii. Glicksman. Rogers. Downey. Witherow, Facemire. and Frazier

1008

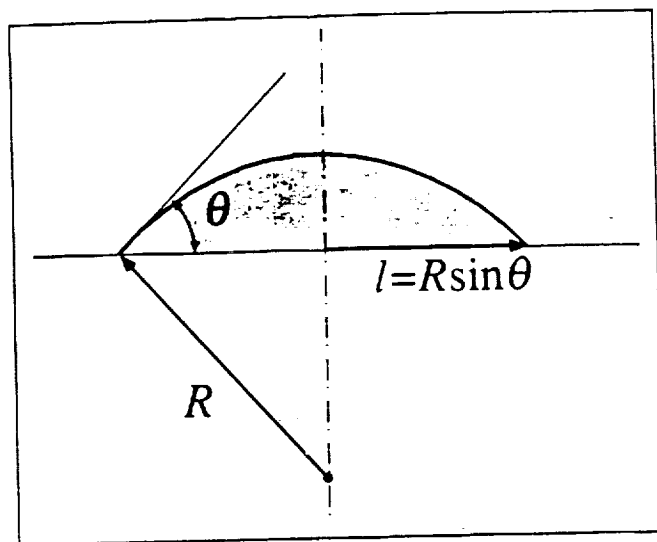Fig. 1. Configuration of a droplet. shaped as a spherical cap. at the experimental cell wall. where l is the visible radius of the droplet and R is the radius of curvature of the droplet.

buoyancy) system. Liquid phase separation in succinonitrile-water alloy below the critical consolute temperature was studied in this experiment. Small (10 to 50 μm) droplets of one liquid were dispersed in the other, attaining uniform shapes of spherical caps, as a precipitate on the walls of the test cell. An isothermal four-month-long anneal permitted extensive coarsening via diffusion among the precipitated droplets. The distance between the front and the back cell walls is 100 μm, which is smaller than the typical distance between the droplets. The boundary conditions at the walls impose a zero normal diffusion flux. Such geometry and the boundary conditions, often characteristic of coarsening in thin films. imply that the diffusion flux in the direction normal to the walls is much smaller than the flux in the direction parallel to the walls. Thus, in the theoretical formulation, the diffusion field among the three-dimensional droplets is considered as two-dimensional.

This paper presents the mathematical treatment for the mixed-dimensional coarsening system studied in Ref. 1. The theory is developed, using a multipolar series expansion. Two approximate solutions are discussed, which are monopolar and dipolar. The results of the respective calculations are compared with each other and with the experimental data.

GENERAL FORMULATION

The theoretical analysis of coarsening of droplets requires solving a moving boundary diffusion problem (Stefan problem) with boundary conditions applied at the test cell walls and at the surfaces of the droplets. The boundary condition imposed on the curved droplet surfaces is given by the usual linear form of the Gibbs-Thomson equilibrium equation, namely

$$c(R) = c_0 \left(1 + \frac{L}{R} \right), \qquad (1)$$

where $c(R)$ is the equilibrium concentration at the surface of the droplet with radius R. c_n is the equilibrium concentration at a planar interface, and L is the Gibbs-Thomson characteristic length, given by

$$L = \frac{2\gamma\Omega}{kT}, \qquad (2)$$

where γ is the interfacial tension, Ω is the molecular volume. k is the Boltzmann constant, and T is the temperature. A typical value for L is 10^{-7} cm.

A numerical solution of this problem appears unrealistic for a large number of droplets. However, if the supersaturation is low, then the characteristic diffusion time is much shorter than the time needed for a significant change of the droplet radius. As a consequence. the diffusion equation,

$$\frac{\partial c}{\partial t} = D\nabla^2 c, \qquad (3)$$

reduces to the Laplacian equation,

$$\nabla^2 c = 0. \qquad (4)$$

This concept was originally suggested by Todes,[2] and applied later by Lifshitz and Slyozov,[3] Wagner,[4] and many others. The rate of change of droplet size is given by

$$\frac{d}{dt}\left(\frac{4\pi}{3} \alpha(\theta) \cdot R^3 \right) = \Omega D \oint_{\substack{\text{droplet}\\ \text{surface}}} \nabla c \, dS \qquad (5)$$

where α is a geometrical factor relating to the droplet volume that depends on the contact angle, θ (see Fig. 1), of the droplet,[5]

$$\alpha(\theta) = \frac{1}{4}(2 - 3\cos\theta + \cos^3\theta). \qquad (6)$$

The boundary conditions at the test cell walls result in the replacement of the three-dimensional diffusion problem by a two-dimensional one, neglecting the diffusion flux across the cell walls compared to the flux along the walls. In the resulting two-dimensional formulation of the problem, the surface integral in Eq. (5) is rewritten as a contour integral along the visible droplet perimeter s:

$$\frac{d}{dt}\left(\frac{4\pi}{3} \frac{\alpha(\theta)}{\sin^3\theta} \cdot l^3 \right) = \Omega DH \oint_{s} \nabla c \, ds, \qquad (7)$$

where H is the distance between the test cell walls, l is the visible radius of the droplet shown in Fig. 1, related to the spherical radius of the droplet (radius of curvature) as $l = R\sin\theta$. From here on, we will use l rather than R, because l is the only measurable characteristic of the droplet size in the experiment.[1]

Even after this simplification. the problem still remains too difficult for direct numerical analysis. Each droplet surface represents a continuum of sources/sinks for solute atoms. Insofar as the concentration field obeys the Laplacian Eq. (4), one may use a multipole series expansion to approach the exact

boundary conditions at the droplet surfaces, assuming that the interdroplet distance is much larger than the visible droplet radii. In two dimensions, the concentration as a function of location $\bar{r}$ is given as

$$c(\bar{r}) = c^* + c_0\left(-q \ln r + \frac{\bar{d}\cdot\bar{r}}{r^2} + ...\right),\quad (8)$$

where scalars c^* and q, and vector $\bar{d}$ are the constants of integration to be determined using the boundary conditions.[6] Employing the electrostatic analog of quasi-static diffusion, one finds that q corresponds to an isolated charge, and $\bar{d}$ corresponds to a dipole moment. The larger the interdroplet distance as compared to the droplet radii, the fewer terms of the series required. The logarithmic term is referred to as the two-dimensional monopole term, the next as the dipole term, etc. It is important to mention that the rate of the visible droplet size change is defined by the monopole term alone:

$$\frac{d}{dt}l_i = -\frac{\sin^3\theta}{2\alpha(\theta)}\Omega\cdot Dc_0 H\frac{q_i}{l_i^2}.\quad (9)$$

Introducing the dimensionless potential φ instead of the concentration c as

$$\varphi = \frac{(c-c_0)}{c_0}.\quad (10)$$

Eq. (4) can be rewritten as

$$\nabla^2\varphi = 0\quad (11)$$

The theory is first developed by neglecting terms higher than the monopole, and then incorporating the dipole terms. The general two-dimensional solution of the Laplacian equation in the monopole approximation is

$$\varphi(\bar{r}) = \varphi^* - \sum_{i=1}^N q_i \ln\frac{|\bar{r}_i - \bar{r}|}{a},\quad (12)$$

where $\bar{r}_i$ is the position of the center of the i-th droplet, a is an arbitrary constant with dimensionality of length, and $\varphi^* = (c^* - c_0)/c_0$. The Gibbs-Thomson boundary conditions (1) are used to obtain the values of $(N+1)$ constants of integration, viz. φ^* and q_i. Neglecting the visible droplet radius as compared to the interdroplet distance, one can substitute the position at the surface of the droplet by the position of its center. This results in a linear set of N equations

$$\frac{L\sin\theta}{l_i} = \varphi^* - q_i \ln\frac{l_i}{a} - \sum_{j\neq i} q_j \ln\frac{|\bar{r}_i - \bar{r}_j|}{a}.\quad (13)$$

The reference experiment, see Part I,[1] showed that the total volume of the droplets did not depend on time during the isothermal annealing (see Fig. 2). Mass conservation, which can be written in terms of the q_i's using Eq. (9) is expressed as

$$\sum_{i=1}^N q_i = 0,\quad (14)$$

and provides the last equation needed to complete the set. As a consequence of Eq. (14), the constant a in Eq.

(13) cancels out, and its value does not effect the solution. We will choose $a = L\sin\theta$.

The monopole approximation neglects the size of the droplets, and does not account for the gradients of the diffusion field in the vicinity of the droplets. Note, that in two dimensions the monopole term, a logarithmic function, changes very slowly. The next term in the expansion is the dipole term, which accounts for the gradients in the vicinity of droplets. This term decays as the reciprocal of distance. The higher order terms, which decay faster than the dipole term, are neglected.

The general solution of the Laplacian Eq. (11) incorporating the dipole terms is given by

$$\varphi(\bar{r}) = \varphi^* - \sum_j\left(-q_j\ln\frac{|\bar{r}-\bar{r}_j|}{L\sin\theta} + \frac{\bar{d}_j\cdot(\bar{r}-\bar{r}_j)}{|\bar{r}-\bar{r}_j|^2}\right)\quad (15)$$

The boundary conditions at the surfaces of all droplets are given by

$$\frac{L\sin\theta}{l_i} = \varphi^* - q_i\ln\frac{l_i}{L\sin\theta} + \frac{\bar{d}_i\cdot\bar{l}}{l_i^2}$$
$$+ \sum_{j\neq i}\left(-q_j\ln\frac{|\bar{r}_i-\bar{r}_j|}{L\sin\theta} + \frac{\bar{d}_j\cdot(\bar{r}_i-\bar{r}_j)}{|\bar{r}_i-\bar{r}_j|^2}\right),\quad (16)$$

and hold for $\bar{l}_i$ in any direction, where $\bar{l}_i$ is the vector originating at the center of the i-th droplet and ending at an arbitrary point on its perimeter. The potential field in the vicinity of the i-th droplet created by the rest of the system, φ_i, is given by

$$\varphi_i(\bar{w}) \equiv$$
$$\varphi^* + \sum_{j\neq i}\left(-q_j\ln\frac{|(\bar{r}_i+\bar{w})-\bar{r}_j|}{L\sin\theta} + \frac{\bar{d}_j\cdot((\bar{r}_i+\bar{w})-\bar{r}_j)}{|(\bar{r}_i+\bar{w})-\bar{r}_j|^2}\right)\quad (17)$$
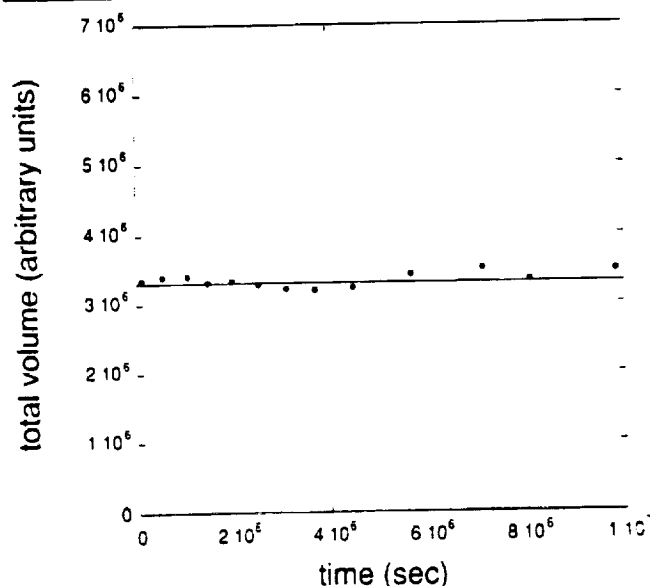
Fig. 2. Total volume of the observed droplets calculated as the sum of their cubed radii vs time.

Fradkov, ι.ι..ni. Glicksman, Rogers, Downey,
Witherow, Facemire, and Frazier

1010

where $\bar{w}$ is a vector originating at the center of the i-th droplet. Rewriting the boundary condition Eq. (16) using Eq. (17) gives

$$\frac{L\sin\theta}{l_i} = \varphi_i(0) - q_i \ln\frac{l_i}{L\sin\theta} + \left.\frac{d\varphi_i}{d\bar{w}}\right|_0 \cdot \bar{I}_i + \frac{\bar{d}_i \cdot \bar{I}_i}{l_i^2}, \quad (18)$$

where

$$\frac{d}{d\bar{w}} \equiv \bar{i}\frac{\partial}{\partial w_x} + \bar{j}\frac{\partial}{\partial w_y}. \quad (19)$$

To satisfy Eq. (18) for any $\bar{I}_i$, the following two equalities must be met:

$$\frac{L\sin\theta}{l_i} - \varphi_i(0) + q_i \ln\frac{l_i}{L\sin\theta} = 0, \quad (20)$$

and

$$\frac{\bar{d}_i}{l_i^2} + \left.\frac{d\varphi_i}{d\bar{w}_i}\right|_0 = 0. \quad (21)$$

The following set of $(3N + 1)$ linear equations for q_i's, $\bar{d}_i$'s, and φ^* result:

$$\left.\begin{array}{l}\displaystyle\sum_{j\neq i}^{N}\left(-q_j\ln\frac{r_{ji}}{L\sin\theta} + \frac{x_{ji}d_{x_j}}{r_{ji}^2} + \frac{y_{ji}d_{y_j}}{r_{ji}^2}\right) \\[4mm] -q_i\ln\frac{l_i}{L\sin\theta} + \varphi^* = \frac{L\sin\theta}{l_i} \\[4mm] \displaystyle\frac{d_{x_i}}{l_i^2} - \sum_{j\neq i}\left(-\frac{x_{ji}}{r_{ji}^2}q_j + \frac{r_{ji}^2 - 2x_{ji}^2}{r_{ji}^4}d_{x_j} - \frac{2x_{ji}y_{ji}}{r_{ji}^4}d_{y_j}\right) = 0 \\[4mm] \displaystyle\frac{d_{y_i}}{l_i^2} - \sum_{j\neq i}\left(-\frac{y_{ji}}{r_{ji}^2}q_j - \frac{2y_{ji}x_{ji}}{r_{ji}^4}d_{x_j} + \frac{r_{ji}^2 - 2y_{ji}^2}{r_{ji}^4}d_{y_j}\right) = 0 \\[4mm] \displaystyle\sum_{j=1}^{N}q_j = 0\end{array}\right\} \quad (22)$$

where $x_{ji} = x_i - x_j$; $y_{ji} = y_i - y_j$; $r_{ji} = \sqrt{(x_i - x_j)^2 + (y_i - y_j)^2}$.

DIMENSIONLESS FORMULATION

Using the Gibbs-Thomson characteristic length L as a length scale $L\sin\theta$ as a unit of length, dimensionless variables are introduced for convenience: the dimensionless droplet size

$$\lambda_i = \frac{l_i}{L\sin\theta}, \quad (23)$$

the dimensionless characteristics of the droplet center positions

$$\bar{\rho}_i = \frac{\bar{r}_i}{L\sin\theta}; \xi_i = \frac{x_i}{L\sin\theta}; \eta_i = \frac{y_i}{L\sin\theta} \quad (24)$$

the dimensionless time

$$\tau = \frac{\sin^3\theta}{2\alpha(\theta)}\frac{\Omega Dc_0 H}{L^3\sin^3\theta}t = \frac{1}{16\alpha(\theta)}\frac{Dc_0 Hk^3 T^3}{\gamma^3\Omega^2}t, \quad (25)$$

and the dimensionless dipole moments of the droplets

$$\bar{\delta}_i = \frac{\bar{d}_i}{L\sin\theta}.$$

The monopole moments for two-dimensional diffusion fields are naturally dimensionless.

Using these variables, Eqs. (11) and (22) reduce to

$$\frac{d}{d\tau}\lambda_i = -\frac{q_i}{\lambda_i^2}, \quad (26)$$

$$\frac{1}{\lambda_i} = \varphi^* - q_i\ln\lambda_i - \sum_{j\neq i}q_j\ln|\bar{\rho}_i - \bar{\rho}_j|. \quad (27)$$

$$\left.\begin{array}{l}\displaystyle -q_i\ln\lambda_i + \sum_{j\neq i}^{N}\left(-q_j\ln\rho_{ji} + \frac{\xi_{ji}\delta_{x_j}}{\rho_{ji}^2} + \frac{\eta_{ji}\delta_{y_j}}{\rho_{ji}^2}\right) + \varphi^* = \frac{1}{\lambda_i} \\[4mm] \displaystyle \delta_{x_i} - \lambda_i^2\sum_{j\neq i}\left(-\frac{\xi_{ji}}{\rho_{ji}^2}q_j + \frac{\rho_{ji}^2 - 2\xi_{ji}^2}{\rho_{ji}^4}\delta_{x_j} - \frac{2\xi_{ji}\eta_{ji}}{\rho_{ji}^4}\delta_{y_j}\right) = 0 \\[4mm] \displaystyle \delta_{y_i} - \lambda_i^2\sum_{j\neq i}\left(-\frac{\eta_{ji}}{\rho_{ji}^2}q_j - \frac{2\eta_{ji}\xi_{ji}}{\rho_{ji}^4}\delta_{x_j} + \frac{\rho_{ji}^2 - 2\eta_{ji}^2}{\rho_{ji}^4}\delta_{y_j}\right) = 0 \\[4mm] \displaystyle \sum_{j=1}^{N}q_j = 0\end{array}\right\} \quad (28)$$

where

$$\xi_{ji} = \xi_i - \xi_j; \eta_{ji} = \eta_i - \eta_j; \rho_{ji} = \sqrt{(\xi_i - \xi_j)^2 + (\eta_i - \eta_j)^2}.$$

NUMERICAL TREATMENT

The set of ordinary differential Eq. (26) is solved, using a fourth-order Runge-Kutta algorithm. The values of the q_i's are obtained at each time step by solving the sets of linear dimensionless Eq. (27) and Eq. (28) for the monopole and the dipole approximations, respectively. The disappearance of a shrinking droplet causes a singularity in the coefficient matrix for the equation sets Eq. (27) and Eq. (28). This requires the redefinition of the coefficient matrix by dropping the column and row corresponding to the vanished particle. A variable time-step was used to deal with this situation. The time-step was continually chosen by estimating the shortest droplet lifetime. After each time-step, the droplets smaller than a threshold size were eliminated, which allowed the coefficient matrix to be redefined before the singularity occurred. This threshold value was chosen to be much smaller than the current average droplet size in the system. As a droplet becomes small, it rapidly vanishes. with the shrinking rate $d\lambda_i/d\tau$ increasing as $1/\lambda_i^2$. Therefore, the results are stable with respect to the chosen value of the threshold. The results obtained with a threshold value of 5% of the average droplet size in the system proved to be indistinguishable from those for 2%. within the calculation error, which never exceeded 0.01%. The program was tested and verified using a two-droplet case which has a reasonably simple analytical solution.

The initial configuration for the multi-droplet simu-

lation is taken from the experimental data Part I. The relationship between the experimental time t and the computational dimensionless time τ is found, using the theoretically predicted scaling behavior for three-dimensional domains exchanging atoms via a two-dimensional diffusion field. The dimensionality of the problem suggests the scaling law

$$\bar{R}^4 \propto t, \qquad (29)$$

where $\bar{R}$ is any characteristic linear scale of the system, for example, the average radius of the droplets, and t is the time.[7,8] Since $N\bar{R}^3 = $ const, where N is the number of droplets, Eq. (29) gives the time dependence for the number of droplets N as,

$$N^{-4/3} \propto t \qquad (30)$$
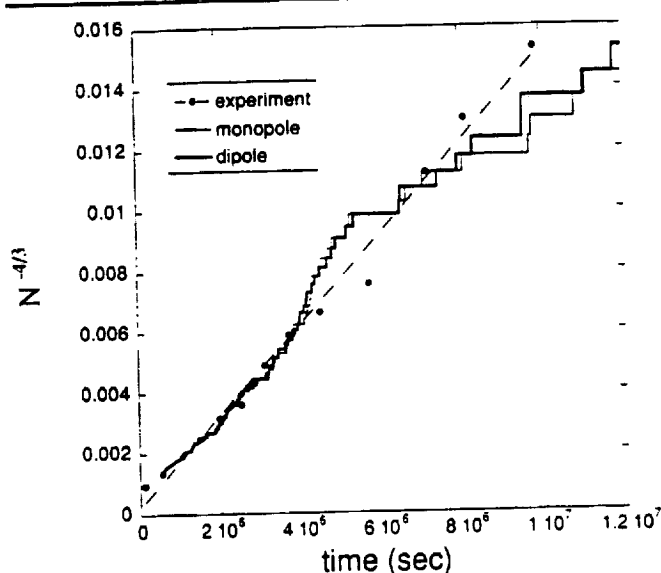
The experimental time dependence of the number of

Fig. 3. Scaling of a number of droplets with time. The initial state for the simulations is the experimental state at t = 540080 s (N = 142).
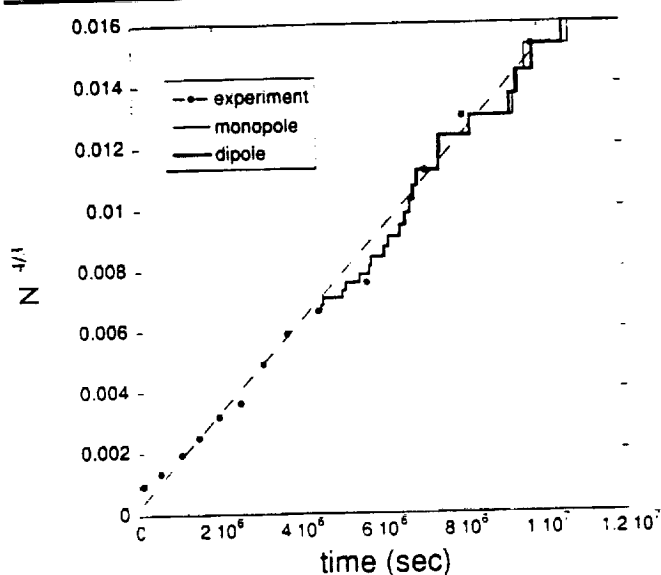

Fig. 4. Scaling of a number of droplets with time. The initial state for the simulations is the experimental state at t = 5697500 s (N = 43).

droplets shown in Fig. 3. The best fit to the numerical calculations for this dependence was obtained for $\tau = 5.9 (t - t_0)$, which gives a value for the combination of parameters appearing in Eq. (25). The time dependence of the number of particles calculated using both monopole and dipole approximations fit the experimental data well for part of the annealing period, after which deviation increases. This disparity between the experimental and the calculated data, observed for larger times, might result from the accumulated influence of the droplets located beyond the experimental field of view. As stated earlier, in two dimensions, the decay of the interaction among the droplets with the distance is rather subtle. Apparently, the effect of unobserved particles accumulates with time, resulting in the increasing deviation between the experimental and the calculated data. Figure 4 shows that the experimental behavior during the later time interval can be reproduced numerically by choosing a later experimental configuration as the initial condition for the simulations.
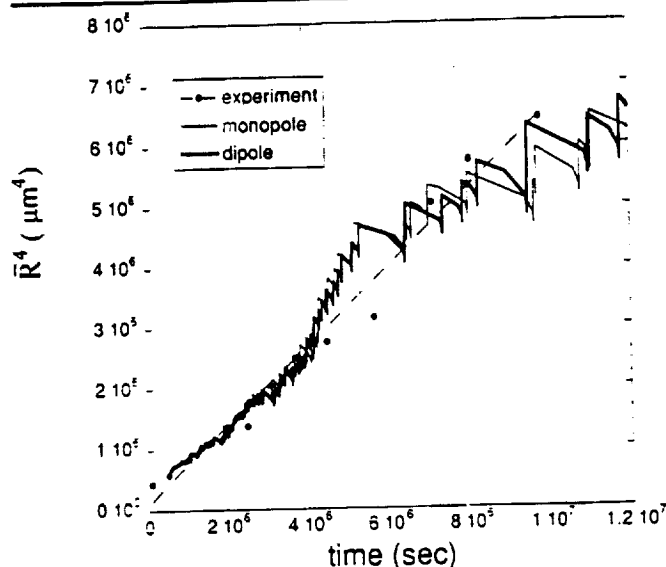
Figure 5 shows the time dependence of the mean

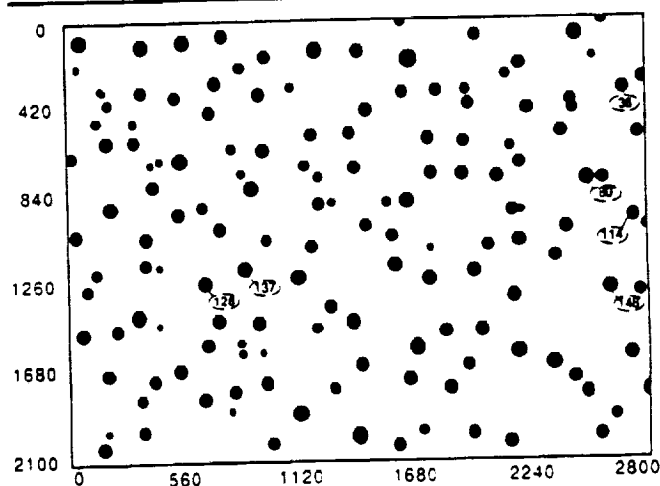Fig. 5. Scaling of the mean droplet radius with time.

Fig. 6. Locations of droplets in the experimental field of view.

Fradkov. .ani. Glicksman. Rogers. Downey.
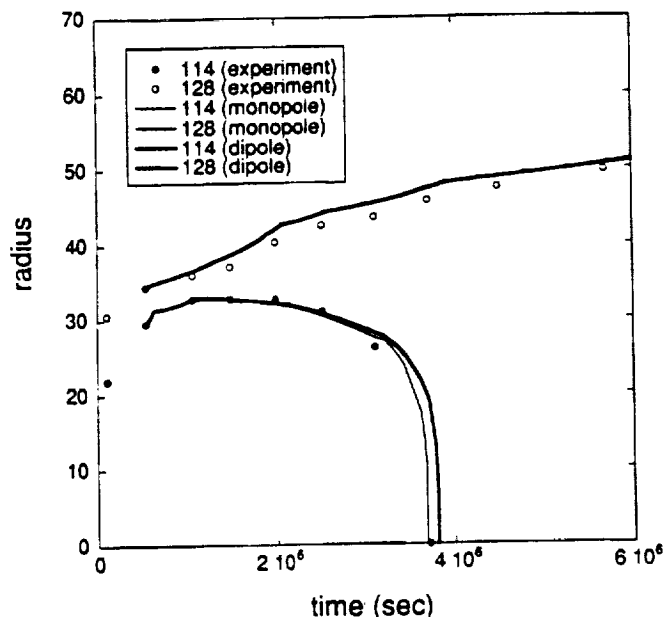Witherow. Facemire. and Frazier

1012

Fig. 7. Typical individual droplet evolution in the case of a good agreement between the experiment and the calculations.
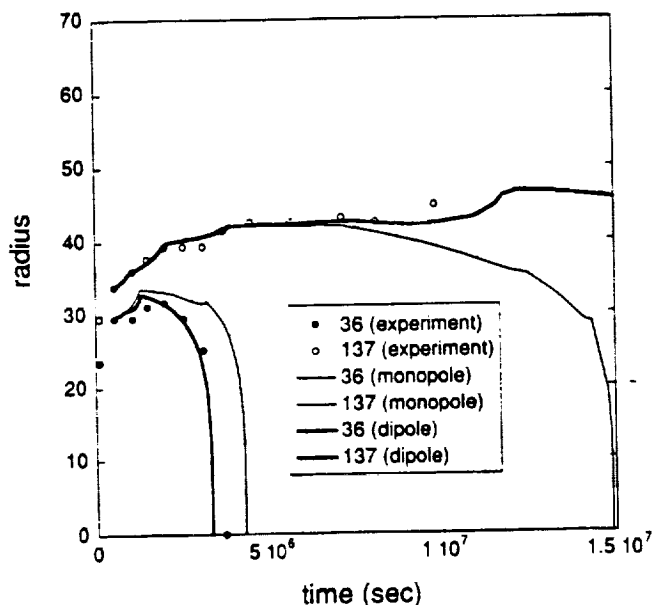

Fig. 8. Typical individual droplet evolution in the case when the dipole approximation shows better agreement with the experiment as compared to the monopole approximation.
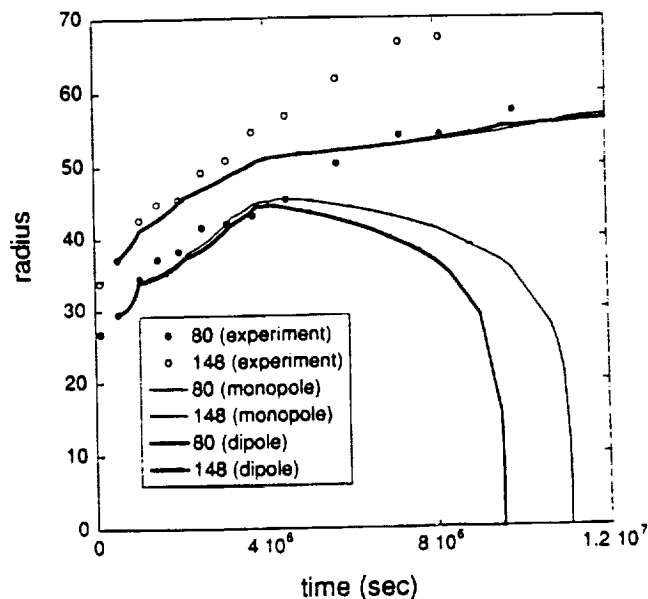

Fig. 9. Typical individual droplet evolution in the case of a bad agreement between the experiment and the calculations.

In contrast with the global behavior, the results of the comparison between the experimental behavior and the calculations for individual droplet evolution vary widely in accuracy. The individual droplet evolution can be categorized in three distinguishable cases. The locations of the representative droplets are shown in Fig. 6. In certain locations, the droplets exhibit good agreement between the experiment and both dipole and monopole approximations, as shown in Fig. 7. For some other droplets, the dipole calculation deviates from the monopole calculation, but the dipole results are in better agreement with the experimental measurements (see Fig. 8). In the third group, deviations are found among the experimental results for both calculations (see Fig. 9). As the only difference between the monopole and the dipole approximations is that the latter incorporates concentration gradients, the particles exhibiting different behavior in the two simulations are located in a strong concentration gradient resulting from the surrounding environment. The cases without agreement between the calculations and the experiment appears to be caused by the uncontrollable influence of droplets located beyond the experimental field of view.

CONCLUSIONS

Theoretical modeling of coarsening among a finite cluster of precipitated droplets between two closely spaced cell walls is performed based on a multipole expansion method. This model calculates the time dependencies of individual droplet radii, given the droplet locations. The theory uses a global mass balance equation rather than an external boundary condition, therefore avoiding the introduction of any additional arbitrary length scale into the system. Two approximations—monopole and dipole—are studied. An initial experimental configuration is used as the

radius of the droplets for the experiment and the calculations based on both monopole and dipole approximations. The simulation shows discontinuities at the times of droplet vanishings. Note that the mean radius decreases between two consequent vanishings. This happens due to phase volume redistribution from the smaller particles shrinking fast, to the larger ones growing slower. However, the mean radius suddenly increases at the instant of a droplet vanishing, exhibiting the expected overall increase in the average. The more droplets present in the system, the smoother is the time dependence of the mean radius.

initial condition for the calculation. Good agreement is observed between the experimental data for the statistically measured parameters, which are the total number and the mean size of the droplets. However, for larger times certain deviations develop, resulting from accumulation of the effects of droplets located beyond the experimental field of view.

The individual droplet evolution compared among the two approximations and the experiment can be categorized in three groups. The droplets in the first group exhibit similar behavior in the experiment and both approximations. The second group displays some deviations between the monopole and the dipole approximations, with the dipole approximation results being in better agreement with the experiment. The monopole approximation accounts for the concentration field, whereas the dipole approximation, additionally, incorporates effects from the concentration gradients resulting from the asymmetrical environment. The third group does not show agreement between any of the approximations and the experiment, apparently due to the limited extent of knowledge of the environment, i.e. the unknown locations and sizes of the particles beyond the experimental field of view.

The multipolar approach explicitly requires that the characteristic interdroplet distance is large as compared to individual droplet sizes, which limits their application to low volume fractions of the dispersed phase. For systems with a high volume fraction, this fundamental assumption fails. Hence, the multipole approach cannot be extended to systems with high volume fraction by merely incorporating additional higher-order terms of the multipolar series. A fundamentally different approach appears to be required for modeling systems with high volume fraction of the dispersed phase.

REFERENCES

1. J.R. Rogers et al., *J. Electron Mater.* 23. 999 (1994).
2. O.M. Todes, *J. Phys. Chem. (Sov.)* 20 (7), 629 (1946).
3. I.M. Lifshitz and V.V. Slyozov, *J. Phys. Chem. Solids* 19, 35 (1961).
4. C. Wagner. *Z. Electrochem.* 65, 581 (1961).
5. B.K. Chakraverty, *J. Phys. Chem. Solids* 28, 2401 (1967).
6. L.D. Landau and E.M. Lifshitz, *The Classical Theory of Fields,* 4th rev. English ed. (Oxford. New York: Pergamon Press, 1975).
7. W.W. Mullins. *J. Appl. Phys.* 28 (3), 333 (1957).
8. V.V. Slyozov. *Sol. State Phys.* (Sov) 9. 927 (1967).